Acetylcholine receptor channel imaged in the open state

Nigel Unwin

MRC Laboratory of Molecular Biology, Hills Road, Cambridge CB2 2QH, UK

The structure of the open-channel form of the acetylcholine receptor has been determined from electron images of *Torpedo* ray postsynaptic membranes activated by brief (<5 ms) mixing with droplets containing acetylcholine. Comparison with the closed-channel form shows that acetylcholine initiates small rotations of the subunits in the extracellular domain, which trigger a change in configuration of α-helices lining the membrane-spanning pore. The open pore tapers towards the intracellular membrane face, where it is shaped by a 'barrel' of α-helices having a pronounced right-handed twist.

THE brain functions by sending electrical signals across different synapses connecting cells of the nervous system. Neurotransmitter-gated ion channels, of the acetylcholine (ACh) and glutamate receptor families, are the protein molecules in the postsynaptic membranes that control the rapid propagation of these signals between most cells. The fast-acting channels open transiently upon stimulation by the neurotransmitter and ions flow through them down their electrochemical gradients, leading to a change in membrane potential. How the opening is accomplished is not known, yet is fundamental to our understanding of synaptic communication.

The nicotinic ACh receptor, a 290K protein at the nerve–muscle synapse, is the most thoroughly studied neurotransmitter-gated ion channel[1–4]. It consists of a ring of five similar subunits ($\alpha\alpha\beta\gamma\delta$), delineating through the membrane a central pathway for the ions. The pathway is narrow across the membrane, but widens into a ~20 Å diameter cylinder that extends ~65 Å into the synaptic cleft and ~15 Å into the interior of the cell[5–7]. The narrow, membrane-spanning portion, the pore, is lined by five α-helical segments, M2, one from each of the polypeptide chains[2,4]. These segments in the absence of ACh appear to come together near the middle of the membrane and form the gate of the channel[7]. The gate opens upon binding of ACh to distant sites on the two α-subunits, and closes again when ACh is depleted from the synaptic cleft or when, in the continued presence of ACh, desensitization occurs. The muscle-type channels desensitize quickly (time constant: ~50–100 ms at 20–22 °C)[8,9] but slowly compared to their opening rate (time constant: ~20 μs)[9–11], and achieve close to a 100% probability of being open during initial activation with high concentrations of ACh[8–11].

Recently it has become possible to record images of ACh receptors, in which the open-channel form should predominate, by mimicking the initial transient activity at the synapse. The experiment (Fig. 1) involves brief mixing of spray droplets containing ACh with isolated postsynaptic membranes; rapid freezing to trap the structural response; and electron microscopy of the frozen membranes. I describe here the structure of the channel at 9 Å resolution, determined from the images after such activation and trapping, and compare it with the structure of the closed channel determined earlier at the same resolution[7]. The map reveals an altered configuration of M2 α-helical segments, encircling an open pore, and localized disturbances at the presumed level of the two ACh binding sites which are communicated to the membrane-spanning portion through small rotations of the subunits.

Millisecond mixing and freezing

ACh receptor-rich postsynaptic membranes were obtained from the muscle-derived electric organ of the *Torpedo* ray. The membranes, after isolation and resuspension in a low-salt solution, crystallize in the form of long tubular vesicles[12]. These tubes are composed of receptors, peripheral proteins and lipid molecules arranged on a p2 surface lattice in an outside-out orientation (Fig. 2*a*). A single image of a tube allows a complete three-dimensional structure to be determined, because the tube has overall helical symmetry[13].

An atomizer spray coupled to a rapid freezing device was developed to achieve ACh-receptor reaction times of less than 5 ms at 5 °C (ref. 14), in order to trap the open channels and minimize desensitization. Solutions containing the tubes were applied to holey carbon support grids, which were blotted to produce thin aqueous films and plunged by free-fall into ethane cooled by liquid nitrogen. Spray droplets, containing 100 mM ACh and ferritin marker particles, were made to impinge on the grids 5 ms before they hit the ethane surface, thus allowing brief mixing with the film contents before the freezing. Tubes were photographed in areas of the frozen films near the edges of the spreading droplets, where the concentration of ferritin particles was typically 1/10–1/100th of the concentration in the spray. The concentration of ACh molecules in these areas would have risen by diffusion[14] well beyond that needed to achieve a high probability of opening (~50 μM)[8,11].

To check that the receptors in the presence of the ferritin had been affected by ACh, their structure was determined from each tube at only 25 Å resolution, and compared to their structure determined earlier from non-activated tubes[7]. Correlation coefficients were calculated between the two sets of densities in successive sections from a tube radius of 260 Å to 380 Å, corresponding to different levels along the receptor's length. With all such ACh-exposed tubes, the coefficients were highest when there were small, but reproducible, rotations between the two maps (Fig. 2*b*, filled circles). The rotations were smaller and of a different nature to those obtained from desensitized receptors in tubes exposed for several seconds to ACh (Fig. 2*b*, empty circles); no systematic effect could be detected from tubes with ferritin only present in the spray (data not shown). Therefore, the brief exposure to varying concentrations of ACh before freezing had induced a consistent and unique structural change, as would be expected if a high proportion of receptors had been trapped in the open-channel form.

Each of 28 tubes imaged in the vicinity of the spreading droplets yielded a set of Fourier terms extending to a resolution of 9 Å. These terms were averaged to improve the signal to noise ratio, as in the earlier structure determination from non-activated tubes[7]. In both structure determinations (Table 1), the averaging was done on >50,000 molecules, using tubes of the same helical family imaged under the same conditions (see legend to Fig. 2 for details). Comparable errors in the phases, over successive resolution zones (see legend to Fig. 2), demonstrated

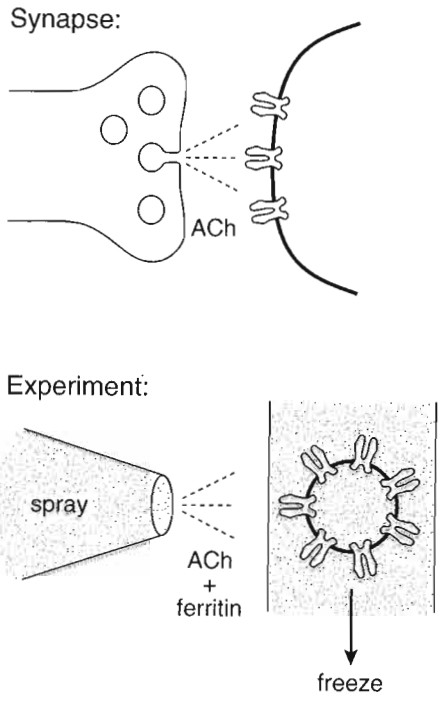

FIG. 1 Channel-opening event at the synapse (above) and the experiment to capture this event *in vitro* (below). In the experiment, the spraying of ACh-containing droplets onto an aqueous film containing isolated postsynaptic membranes (tubular vesicles) mimics the release of neurotransmitter onto the target cell, and rapid freezing traps the channels in the open state. Ferritin marker particles, included in the spray solution, reveal the regions of the film where the droplets have impinged and spread, and so identify the membranes containing open channels.

that the activation did not introduce appreciable loss of crystallinity.

Channel mouth

A 9 Å map of the ACh-activated receptor was calculated from the averaged Fourier terms in sections normal to the axis of the channel, and then compared to the map of the non-activated receptor[7]. The two structures are most alike at the extracellular mouth of the channel: from the tips of the subunits to about a third of the way down towards the membrane (Fig. 3*a*, *b*). Within this region, the water-facing surfaces match fairly closely, and the two sets of densities are more similar (mean correlation coefficient: 0.91) than elsewhere in the receptor. Extensive subunit–subunit contacts are made at the channel mouth, which may limit the possibilities for rapid conformational change.

The two structures show greater differences beginning ~45 Å from the membrane, slightly above the region (A, Fig. 2*b*), where the ACh-binding sites are thought to be located[7,15,16], continuing along the shaft (S, Fig. 2*b*) connecting this level to the membrane, and around the pore itself. The disturbances, initiated at the ACh-binding sites and propagated to the membrane, appear as small net displacements around the channel axis at low resolution, which correlate with the negative–positive rotations indicated in Fig. 2*b*.

ACh-binding sites

The ACh-binding sites in the α-subunits are not equivalent, because they are shaped partly by the neighbouring γ- or δ-subunits[17–20] and have different affinities for ACh[21,22]. In the non-activated structure at the presumed level of these sites, the α-subunits were seen to contain sets of three rods of density, typical of α-helices, running roughly normal to the membrane plane[7]. The other subunits shared these features. However, unique to both α-subunits at the centres of the set of rods were equal-sized cavities, which may be the actual ACh-binding pockets[7]. In the activated structure, the α-subunit next to the δ-subunit, α_δ, is noticeably altered because the cavity it had has disappeared; otherwise, corresponding subunits have similar individual features in the two maps.

Figure 3*c* is a cross-section through the activated structure at the presumed level of the binding sites, with peaks in the contours indicating the positions of the rods, and crosses marking the former positions of the two cavities, only one of which (in α_γ) is still visible. At α_δ, where the cavity has disappeared, the encircling peaks are displaced anticlockwise from their former positions (blue spots). If the peaks are traced at successive levels to give a three-dimensional picture (Fig. 3*d*), and compared to the former traces (Fig. 3*d*, inset), it is seen that these displacements originate from a concerted twisting of the rods. The largest changes are above the (former) cavity, where each rod has rotated anticlockwise by up to ~28°. Smaller changes in the positions of the rods, beneath the cavity, appear to initiate a small clockwise rotation of the subunit that continues down to the membrane (see below).

The localized twisting in α_δ displaces the rods circumferentially, and so must affect the neighbouring subunits. Indeed, it can be shown that this disturbance is part of a coordinated change in the vicinity of the binding sites by comparing the two structures in sectors of 72° (rather than 360°, as before), centred over successive subunits. The sector comparison indicates that the disturbance at α_δ contributes the most to the varying rotational disparities between sections around this level in Fig. 2*b*, and that the effects diminish going anticlockwise around the ring (Fig. 2*b*, box). In contrast, the β-subunit (between the

TABLE 1 Crystallographic data

	−ACh	+ACh (<5 ms)
Number of tubes*	26	28
Receptors	55,000	51,100
Resolution (Å)	8.7	8.7
Defocus range (Å)	7,000–18,800	6,200–16,400
Layer-lines	230	234
Fourier terms	9,126	9,022
2-Fold phase error (°)†	10.6	12.4

* All tubes have (−16, 6) helical symmetry[6,7]; the p2 surface lattice has dimensions: $a = 80.2$ Å, $b = 145.5$ Å, $\gamma = 114.0°$ (at tube radius: 290 Å).

† Amplitude-weighted phase error against 0° or 180°; see also legend to Fig. 2.

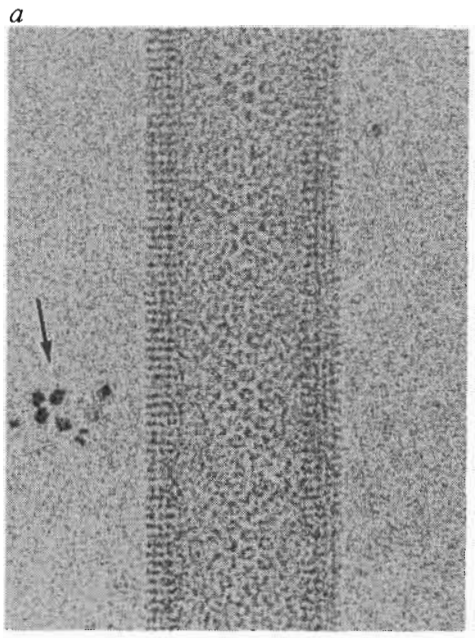

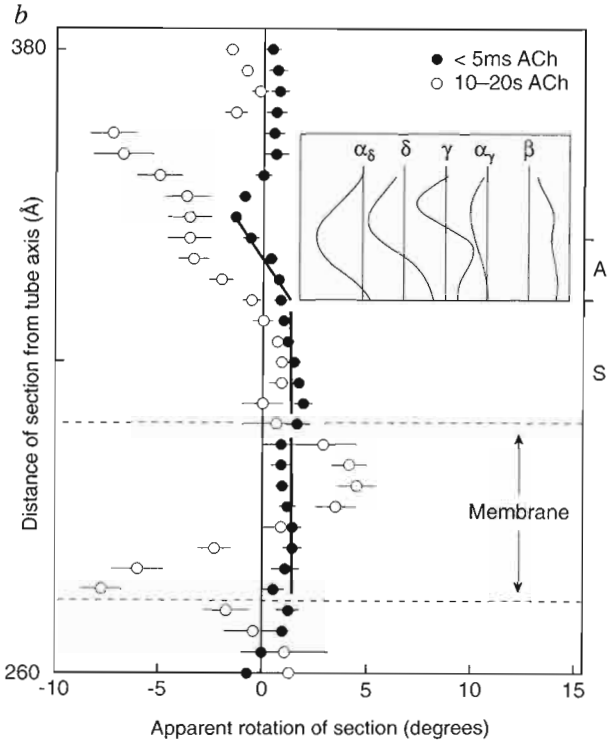

FIG. 2 *a*, Postsynaptic membrane 'tube' after the spray-mixing and freezing, imaged at −178 °C. Crystalline arrays of ACh receptors are visible on the tube surface, contrasted darkly against the surrounding lipid and ice. The extracellular domains of the receptors face outwards, giving the edge of the tube a striated appearance. The presence of ferritin particles (arrow) in the vicinity of the tube indicates that the area is near the edge of a spreading droplet, and that the receptors have therefore been exposed to ACh. The tube diameter is 760 Å. *b*, Structural changes in the ACh receptor after spray-mixing and freezing (filled circles), and prolonged application of ACh to induce desensitization (unfilled circles), detected at 25 Å resolution in three-dimensional maps from individual tubes. Each map was compared, section by section at 4 Å intervals, with the map of the receptor determined from non-activated tubes[7]. Shown are the rotations required to give maximum correlations between sections at successive levels along the receptor's length (extracellular end uppermost), measured from the central axis of the tube. The data were obtained from 37 maps (sprayed tubes) and 8 maps (tubes to which 5 mM ACh had been added 10–20 s before freezing); the bars are standard errors of the mean. A denotes the level of the ACh binding sites and S the level of the shaft connecting this level to the membrane. Lines drawn through the datapoints emphasize distinct disturbances, initiated by ACh, at the levels of the ACh-binding sites, the shaft and the membrane. The box compares the results obtained by correlating the densities in sectors of 72° (also at 25 Å resolution) to show how the net rotational differences at level A (and slightly above) are distributed among the individual subunits, going anticlockwise around the ring; the scales for each subunit, either side of the vertical lines, are as in the main figure.

METHODS. Tubes were suspended in 100 mM sodium cacodylate, pH 6.8, and sprayed with 100 mM acetylcholine chloride and 2 mg ml^{-1} ferritin at the same pH. The tube suspension was applied in 5 μl aliquots to glow-discharged holey carbon films, supported on rigid 300 mesh grids. Rapid freezing was accomplished by a guillotine-type plunger, situated in a cooled high humidity environment, using liquid ethane (at ~−160 °C) as the coolant. Excess solution was blotted off the grid from the side opposite that to which it was applied, and then the grid was plunged by free-fall into the liquid ethane. The plunger incorporated an atomizer spray[14] to deliver a pulse of ~1 μm diameter droplets onto the falling grid. The spray pulse was activated by a photodiode sensor, which detected the displacement of the plunger shaft. The release point of the grid was 35 mm above the nozzle, which was 4 mm above the surface of the ethane, giving 5 ms maximum reaction time between the ACh and the receptors. The temperature of the reaction was 5 °C, measured by a thermocouple attached to a falling grid. Grids were stored in liquid nitrogen and examined within 1.5 years of freezing, using a Gatan cryoholder and a Philips EM420 electron microscope equipped with a low dose kit and operating at 120 kV. Images were recorded at X36,000, of tubes lying within holes in the carbon support film. The electron dose for each image was ~6 electrons per $Å^2$, and a wide range of underfocus was used to ensure that all spacings, at 7% amplitude contrast[46], were well sampled[47]. Tubes belonging to the (−16, 6) helical family[6,7], and surrounded by ferritin particles, were selected visually and by the appearance of the layer-lines in their optical diffraction patterns. The presence of ferritin particles was an important requirement, in addition to the criteria discussed earlier[7]: no effect of ACh (Fig. 2*b*) could be detected in regions of tubes located further than ~1 μm from the nearest ferritin particle. Selected tubes were densitometered and analysed further by computer, essentially as in ref. 7. Briefly, the Fourier terms were obtained along the layer-lines extracted from stretches of tubes equal to integral multiples of the repeat distance; layer-lines from the different stretches were then merged to the same centrosymmetrical origin, taking account of the different contrast transfer functions and the qualities of the data along the *Z* (tube axis) and *R* (radial) directions from each stretch. The structure was calculated directly, without rescaling the amplitudes to compensate for the fading at higher resolution, by Fourier–Bessel inversion and Fourier synthesis. 5-fold averaging was done to obtain the best estimate of the structure common to all five subunits in the membrane-spanning region; as before[7], only one pore-lining rod could be resolved in each subunit before the averaging; no significant non-5-fold feature could be detected in this portion of the receptor. The final dataset was derived from 37 stretches along 28 sprayed tubes. A plot of the sum of the moduli of the contrast transfer functions, from the 28 images, was almost identical to the plot obtained from the non-activated tubes[7]. The overall amplitude-weighted phase error: $\sum|F|\delta\phi/\sum|F|$ (where $\delta\phi$ is the difference between the observed phase and the symmetry-imposed phase of 0° or 180°) was 12.4°. The errors obtained from layer-lines assessed in annular zones of increasing resolution were: 3.5° (68.0–34.5 Å); 8.6° (24.5–22.8 Å); 15.4° (22.8–17.0 Å); 29.1° (17.0–13.7 Å); 31.1° (13.7–11.4 Å); 31.8° (11.4–9.8 Å); 31.9° (9.8–8.7 Å); the corresponding figures for the non-activated structure were: 2.9°; 6.2°; 13.9°; 23.0°; 24.5°; 30.4°; 35.1°, with roughly the same number of measurements (>120) made in each zone.

α-subunits; but see legend to Fig. 3) contributes nothing to the varying rotational disparities, and is displaced in the opposite sense to α_δ. The β-subunit is therefore the least flexible in the vicinity of the binding sites and, instead of deforming, moves away from α_δ. This movement, in Fig. 3*c*, has led to small shifts in the peaks in density away from their former locations, following the direction of the arrow.

ACh induces a similar disturbance in α_γ as in α_δ (Fig. 2*b*, box), but affects this subunit more weakly, presumably because α_γ is tightly coupled to the β-subunit. On the basis of the

details just described, it seems that the tight coupling and imposed rigidity have together enabled the disturbance initiated at α_γ to draw the β-subunit away from α_δ (arrow, Fig. 3*c*), opening up the structure to allow the twisting. This combined action coordinates the structural responses of the two α-subunits, and so is likely to be central to the cooperative mechanism of channel opening[22]. However, the ACh molecule itself and other fine features have not been resolved, and Fig. 2*b* indicates that the interactions at this level are quite complex.

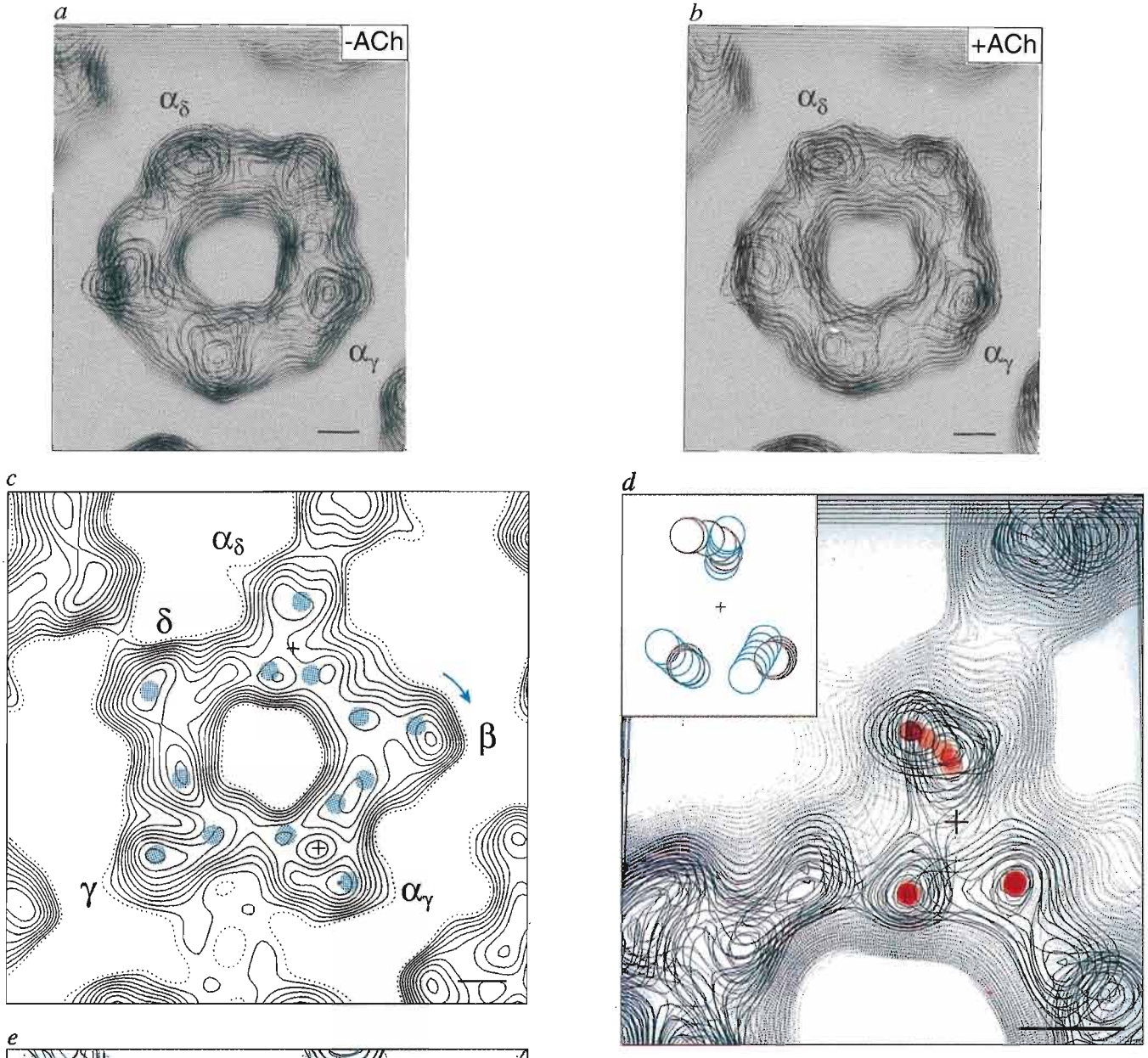

FIG. 3 Extracellular domain. *a*, *b*, Views from the synaptic cleft of the mouth of the channel before (*a*) and after (*b*) activation by ACh, made by stacking successive 2 Å-spaced sections on top of one another; *c*, Section through the ACh-binding region (tube radius: 336 Å), showing positions of peaks of density (corresponding to rods in three dimensions), before (blue spots[7]) and after (contours) activation; crosses mark the centres of the cavities visible before activation[7]; the arrow denotes displacement of the β-subunit away from α_δ (see text); *d*, Detail of the α_δ subunit after activation in a 10 Å thick slab through the putative ACh-binding pocket (tube radii: 330–340 Å; central axis of receptor at bottom); pink disks centred over the peak densities in each section trace the paths taken by the rods; the inset shows the positions of the rods (black circles) relative to their positions before activation (blue circles), viewed normal to the plane of the sections. *e*, Densities projected down a length of the shaft connecting the ACh-binding region to the membrane (tube radii: 316–326 Å) before (blue contours) and after (black contours) activation; clockwise rotations of the α-subunits (arrows) alter the shape of the wall lining the channel. The subunit assignments are based on labelling studies in projection[48], and on three-dimensional features[6,7]. Other lines of evidence suggest that the assignments for γ and β should be interchanged[3]. Scale bars, 10 Å.

Shaft

The shaft is a roughly 25 Å-long region of the receptor, connecting the binding-site region to the membrane-spanning portion in which the subunits appear as distinct columns of density aligned parallel to the axis of the channel[6]. Figure 3*e* compares the activated and non-activated (blue) shaft structures projected down the axis. Small clockwise rotations of the α-subunits (arrows), that appear to be initiated at the binding sites, are propagated down the shaft. These show in Fig. 3*e* as changes in the distributions of the densities composing both α-subunits, and as distortions to the shape of the inner channel wall (which in the non-activated structure is pentagonally symmetrical).

No distinctive secondary structure is resolved in the shaft region of the receptor, so the changes in this region are not as obvious as they are in the vicinity of the binding sites. By isolating the densities composing each subunit in 25 Å diameter cylinders around its centre of mass, and comparing these densities in successive sections down the shaft (beginning 8 Å below the level in Fig. 3*c*), it is found that the α-subunits have to be rotated by $3.8° \pm 0.8$ s.d. (α_δ) and $3.9° \pm 1.1$ s.d. (α_γ) to achieve highest correlations between the two maps (Fig. 3*e*). The same procedure, applied to the other subunits, indicates smaller rotations (<2°), which are, however, also in a clockwise orientation. Thus, the two α-subunits, to which ACh binds to trigger the initial disturbances, also play the primary role in transmitting the effects of these disturbances to the membrane.

Membrane-spanning structure

The membrane-spanning portion of the activated receptor reveals five rods of density, 25–35 Å long, forming a wall around a pore, and a star-shaped outer rim of continuous density, which faces the lipids. The rods and the rim are arranged symmetrically around the pore, consistent with the high sequence homology among the putative transmembrane segments[23]. Figure 4*a* shows these features, after imposing 5-fold symmetry to obtain the best estimate of the structure common to the subunits. The rods can be identified with the α-helical stretches of amino acids, M2, because they are exposed to the lumen of the pore throughout their length[2,4]. The rim of continuous density seems most likely to be composed of β-sheet according to its appearance[7]; other recent measurements have interpreted the remaining transmembrane segments to be mainly β-structure and turns[24] or mainly α-helical[25].

The M2 helices bend or 'kink' about their mid-points, and so are arranged differently in the two leaflets of the lipid bilayer. In both leaflets they slope radially (by ~12°) towards the axis of the pore, but in the lower (intracellular) leaflet they are predominantly at a tangent to it (Fig. 4*b*, upper left). Neighbouring helical segments in the upper leaflet also are sufficiently apart

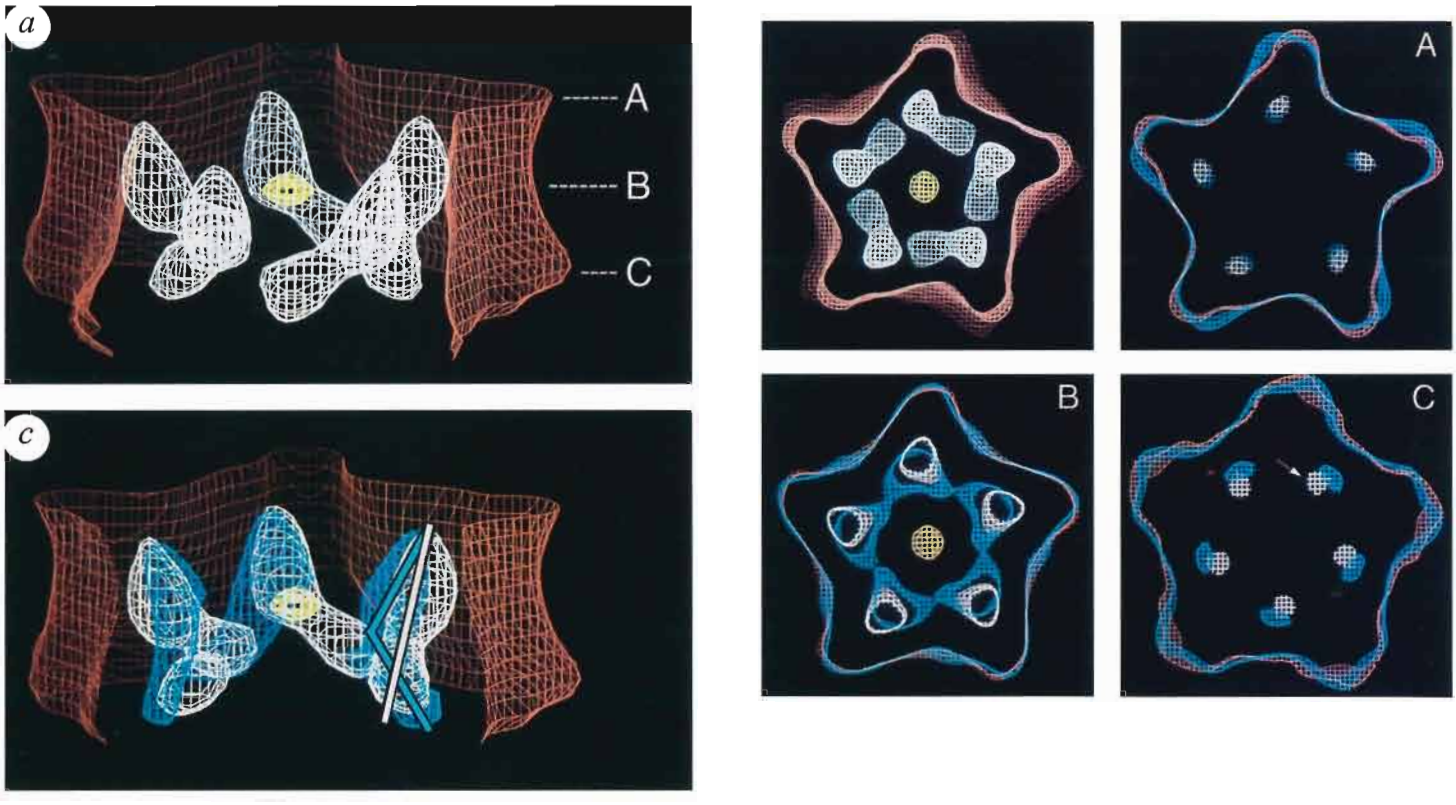

FIG. 4 Membrane-spanning structure. *a*, Open pore showing the M2 helices (white) and the lipid-facing 'rim' (brown); the helical segments bend abruptly near the middle of the membrane and twist around the central axis in the lower (intracellular) leaflet; *b*, Axial view of open pore (upper left) and sections at the levels A, B and C in *a*, comparing details with those of the closed pore (blue): the helical segments of the open pore are tangential to the axis in the lower leaflet (arrow in C), and so have moved the most in this region; *c*, Open pore with the helices of the closed pore (blue) superimposed: the helices around the open pore (white line) are oriented so that they constrict the ion path most at the lower membrane face, whereas the helices around the closed pore (blue line) are oriented so that they point inwards near the middle of the membrane to make the closed gate[7]. The front face of the rim has been removed in *a* and *c* to reveal the helices more clearly. A high-density feature (yellow) on the axis near the middle of the membrane may reflect accumulation of ACh (which acts as a channel blocker at millimolar concentrations[49]) and the proximity at this level of bulky, strongly scattering side-chains. The membrane-spanning portion shown (tube radii: 276–300 Å) corresponds to the hydrophobic core, lying between the phospholipid headgroups[7]. The map grid units correspond to 1 Å (horizontal) and 2 Å (vertical), and the densities are displayed at 50% (rim) and 90% (helices and central feature) of the maximum density.

(up to 21 Å centre-to-centre separation) to allow exposure to the pore of side-chains composing the outer rim, whereas in the lower leaflet they come too close (~10.5 Å centre-to-centre separation) for this to happen, and must be touching one another.

The M2 segments in the intracellular leaflet slope at an angle of ~45° tangential to the axis of the pore. Together they form a 'barrel' of α-helices having a pronounced right-handed twist, that resembles the right-handed barrels of pore-lining α-helices found in the bacterial toxin B-pentamers[26,27], and in heavy riboflavin synthase[28]. However, in the case of the ion channel, it seems likely that the motif is stabilized mainly by contacts around the barrel, with minimal interactions involving residues from the rim. The lower portions of the helices are further from the rim than they are in the closed configuration (see below), and the lower helix residues facing the rim (on the opposite face to those in Fig. 5*c*) are polar. The rigidity of a barrel, combined with a low stability, may be important in ensuring both precise permeation and fast gating kinetics.

Alternative configurations of M2

The structure of the 'open' pore is quite different from that of the closed pore[7], where the helices are also kinked about their mid-points, but come closest to the central axis at the kinks (forming the gate) and slope roughly radially away from the axis above and below that point. Figure 4*b* compares the two structures in sections level with the middle of the membrane and with the two faces (closed pore in blue). The helices making the open pore are further from the axis at the middle of the membrane (B, Fig. 4*b*) and closer to the axis at the lower face (C, Fig. 4*b*). The greatest changes are at the lower face, where the helical segments move across the apex of the star formed by the outer rim to achieve the open pore arrangement (arrow in C, Fig. 4*b*). The rim has the same shape in both structures, suggesting it may act as a framework to partition the moving helices away from the lipids.

These changes in configuration of the helices are linked to a change in orientation of the kinks (Fig. 4*c*). Instead of pointing inwards (closed configuration), they have rotated over to the side, opening up the pore in the region where the gate was located. The rotations are in the same sense as those in the shaft. The kink therefore seems to act as a region of flexure between two α-helical segments, accommodating an extended conformational change. Kinks between α-helical segments have been found to have analogous roles in other proteins[29]. Clearly, the localized flexure provides a simple and effective way of altering the shape, size and environment of the pore.

The ability of the helices to move inside the outer rim seems to be helped by the fact they have two modes of association, neither of which is particularly extensive. The open pore association involves side-to-side interactions around the barrel, whereas the closed pore association involves interactions between exposed side-chains forming a tight central ring[7]. Apparently, these alternative associations reflect equally symmetrical arrangements of the helices around the pore, because the rods of density, after imposing 5-fold symmetry, are resolved with equal clarity in the two maps. There is no indication, in either structure, that the M2 segments contain a stretch of extended polypeptide chain of seven residues[30], but a shorter stretch[31] would be compatible with the abrupt change of angle at the kink.

Ion permeation pathway

The open pore narrows fairly uniformly from the upper to the lower face of the membrane because of a constant radial inclination of the helices of ~12° (as indicated by the line drawn through the helix in Fig. 4*c*). The axes of the helices are about 18 Å from the pore axis at the upper face and 11.5 Å at the lower face, where the pore is most constricted. Assuming the figure of 11.5 Å for the distance of closest approach of the helix to the pore axis, and that hydroxyl-containing residues are projecting directly inwards at this point (see below), the minimum pore diameter would be 9–10 Å. This diameter is only slightly larger than the minimum pore diameter of mouse ACh receptors (8.4 Å)[32], estimated by measurement of their permeability to organic cations of various size. The short extent of the constriction agrees with an estimate of 3–6 Å, based on reversal potential measurements from ACh receptors exposed to osmotic pressure gradients[33].

The uniform narrowing of the open pore towards the lower, N-terminal end of M2 agrees with the results of several types of experiment. Channel blocking reagents, such as chlorpromazine[34,35], triphenylmethylphosphonium[36] and 3-trifluoromethyl-3-*m*-iodophenyldiazarine[37] were found to

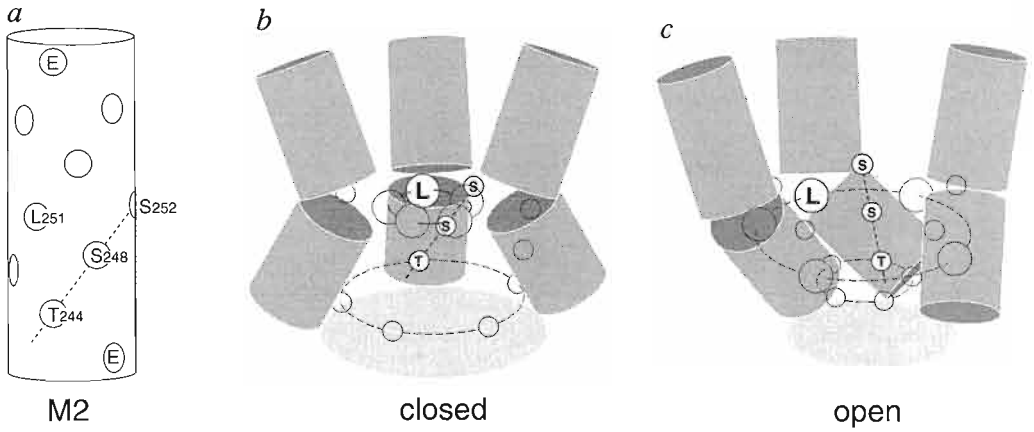

FIG. 5 Pore-lining segment, M2. *a*, Identified pore-facing amino-acid residues[34–41] on an ideal α-helix (6.5 Å radius) viewed from inside the pore; the assignments, E, L251, S252, S248, T244 and E are for the *Torpedo* α-subunit; the glutamic acid residues, E, form part of the 'outer' (upper) and 'intermediate' (lower) rings of negative charge[38]; polar pore-facing residues (serines and threonine) in the lower half of the helix lie at an oblique angle (broken line) to the axis; all subunits have a leucine residue and polar residues at equivalent positions in the sequence. *b*, Closed[7] and *c*, open configurations of M2, with the leucines and polar residues superimposed (see text); relative to *b*, the configuration in *c* has moved back the leucines, reoriented the line of polar residues, and brought T244 (and equivalent residues) closer to the axis of the pore.

penetrate to, and photolabel, residues located in the middle portion of M2, including a highly conserved leucine residue, L251 (refs 35, 37). Mutations reducing the net charge of residues composing the ring of negative charge at the lower end of M2 (E; Fig. 5*a*) were found to affect strongly ion flow, as if this ring is close to the narrowest portion of the pore[38]. An analysis of the influence of mutations on the binding of the open-channel blocker, QX222, indicated that the pore tapers towards the lower end of M2 and drew attention to the likely importance of a line of polar pore-facing residues (S252, S248, T244; Fig. 5*a*)[39]. Mutation of the threonine residue at the bottom of this line (T244) was found either to restrict or enhance ion flow depending on the volume of substituted residue, indicating that this threonine is at, or near to, the point of maximum constriction[40,41].

Alignment of M2 with sequence

The polar pore-facing residues in the lower portion of the ideal α-helix in Fig. 5*a* form a line that slopes by ~40° to its axis at the radius of their hydroxyl groups (6–7 Å). The inclination is similar in magnitude, but opposite in sense, to the slope of the M2 helices in this region of the open pore (Fig. 4*a*). Therefore the line of polar residues should lie almost parallel to the axis of the open pore, an orientation that would aid ion flow by giving optimal exposure of the hydroxyl groups[42]. Furthermore, threonine T244 must be close to the point where the open pore is most constricted[40,41]. Identification of T244 with this level in the structure supports the tentative alignment of the three-dimensional densities with the amino-acid sequence[7], suggesting that L251 is the gate-forming residue projecting from the kink: the kink and the constriction are about 10 Å apart (Fig. 4*c*), and a similar α-helical separation is predicted from the relative positions of these residues in the sequence.

Figure 5*b*, *c* shows the pore-facing residues in alignment with the two configurations of M2, according to the levels indicated for L251 and T244. It had been proposed[7] that the helices, by bending towards the central axis, would allow the large leucine side chains to project inwards and associate in a tight ring, preventing the ions from crossing the membrane (closed pore, Fig. 5*b*); details of the activated receptor now imply that the helices, by bending tangentially to the central axis and associating side-to-side, would allow the polar surfaces to become more fully exposed, while moving the large side-chains away from the ion path (open pore; Fig. 5*c*).

Mechanism of opening

How does ACh weaken the 'leucine-ring' mode of association of the helices (Fig. 5*b*), in favour of their side-to-side association around the barrel (Fig. 5*c*), and open the channel? Although important details have not been resolved, the results of this study suggest some essential elements of the conformational change. First, ACh triggers distinct, localized disturbances at the binding sites in the two α-subunits, which are coordinated allosterically by the single subunit between them. Second, the effects of these disturbances are communicated, through small rotations of the subunits, to the structure in the membrane. Third, the M2 helices in the membrane transmit the rotations to the gate-forming side-chains, drawing them away from the central axis. The ring mode of association is thereby disfavoured, and the helices switch to the alternative side-to-side mode, creating an open pore.

This mechanism would account for the different photolabelling patterns obtained in the presence and absence of agonist[37], suggesting that closely packed hydrophobic residues near the middle of M2 may be 'splayed apart' upon opening. A feature of the channel, once opened, is that it is (weakly) stabilized across the narrow membrane-spanning portion by interactions between the helices around the barrel; so the exact nature of the rotations induced by the ligand are unlikely to be critical as long as they are sufficient to destabilize the gate. These properties may be important in interpreting the strong effects of some mutations involving residues within or (spatially) near to M2 in the ACh receptor[43] and in the homo-oligomeric α-7 nicotinic receptor[44], and the distinct ligand binding and channel specificities of chimaeric receptors having swapped extracellular domains[45].

Conclusion

The experiment reported here, to capture and image the ACh receptor in the open-channel form, has given direct insight into how the receptor works. The confinement of major disturbances to the main functional regions, the development of small rotational motions to disrupt the gate, and the transient formation of an α-helical barrel around the open pore are new principles revealed. Together, they provide a structural basis for explaining the remarkably rapid and efficient response of this synaptic protein to the neurotransmitter, its precise permeation and its almost total impermeability to ions when the neurotransmitter has left[1,8–11,21,32]. It seems likely that other neurotransmitter-gated channels would use similar principles to open their pores and let the ions through. □

Received 12 October; accepted 8 December 1994.

1. Hille, B. *Ionic Channels of Excitable Membranes* (Sinauer, Sunderland, 1992).
2. Lester, H. A. *A. Rev. Biophys. biomolec. Struct.* **21,** 267–292 (1992).
3. Karlin, A. *Curr. Opin. Neurobiol.* **3,** 299–309 (1993).
4. Changeux, J.-P., Galzi, J.-L., Devillers-Thiery, A. & Bertrand, D. *Qt. Rev. Biophys.* **25,** 395–432 (1992).
5. Toyoshima, C. & Unwin, N. *Nature* **336,** 247–250 (1988).
6. Toyoshima, C. & Unwin, P. N. T. *J. Cell Biol.* **111,** 2623–2635 (1990).
7. Unwin, N. *J. molec. Biol.* **229,** 1101–1124 (1993).
8. Dilger, J. P. & Brett, R. S. *Biophys. J.* **57,** 723–731 (1990).
9. Matsubara, N., Billington, A. P. & Hess, G. P. *Biochemistry* **31,** 5507–5514 (1992).
10. Colquhoun, D. & Sakmann, B. *J. Physiol.* Lond. **369,** 501–557 (1985).
11. Colquhoun, D. & Ogden, D. C. *J. Physiol.* Lond. **395,** 131–159 (1988).
12. Brisson, A. & Unwin, P. N. T. *J. Cell Biol.* **99,** 1202–1211 (1984).
13. DeRosier, D. J. & Klug, A. *Nature* **217,** 130–134 (1968).
14. Berriman, J. A. & Unwin, N. *Ultramicroscopy* **56,** 241–252 (1994).
15. Herz, J. M., Johnson, D. A. & Taylor, P. *J. biol. Chem.* **264,** 12439–12448 (1989).
16. Valenzuela, C. F., Weign, P., Yguerabide, J. & Johnson, D. A. *Biophys. J.* **66,** 674–682 (1994).
17. Blount, P. & Merlie, J. P. *Neuron* **3,** 349–357 (1989).
18. Pedersen, S. E. & Cohen, J. B. *Proc. natn. Acad. Sci. U.S.A.* **87,** 2785–2789 (1990).
19. Sine, S. M. & Claudio, T. *J. biol. Chem.* **266,** 19369–19377 (1991).
20. Czajkowski, C. & Karlin, A. *J. biol. Chem.* **266,** 22603–22612 (1991).
21. Jackson, M. B. *Proc. natn. Acad. Sci. U.S.A.* **86,** 2219–2203 (1989).
22. Sine, S. M., Claudio, T. & Sigworth, F. S. *J. gen. Physiol.* **96,** 395–437 (1990).
23. Popot, J.-L. & Changeux, J.-P. *Physiol. Rev.* **64,** 1162–1239 (1984).
24. Gorne-Tschelnokow, U. *et al. EMBO J.* **13,** 338–341 (1994).
25. Blanton, M. P. & Cohen, J. B. *Biochemistry* **33,** 2859–2872 (1994).
26. Stein, P. E. *et al. Structure* **2,** 45–57 (1994).
27. Sixma, T. K. *et al. Nature* **351,** 371–377 (1991).
28. Ladenstein, R. *et al. J. molec. Biol.* **203,** 1045–1070 (1988).
29. Gerstein, M., Schulz, G. & Chothia, C. *J. molec. Biol.* **229,** 494–501 (1993).
30. Akabas, M. H., Stauffer, D. A., Xu, M. & Karlin, A. *Science* **258,** 307–310 (1992).
31. Akabas, M. H., Kaufmann, C., Archdeacon, P. & Karlin, A. *Neuron* **13,** 919–927 (1994).
32. Cohen, B. N., Labarca, C., Davidson, N. & Lester, H. A. *J. gen. Physiol.* **100,** 373–400 (1992).
33. Dani, J. A. *J. Neurosci.* **9,** 884–892 (1989).
34. Giraudat, J. *et al. Proc. natn. Acad. Sci. U.S.A.* **83,** 2719–2723 (1986).
35. Revah, F. *et al. Proc. natn. Acad. Sci. U.S.A.* **87,** 4675–4679 (1990).
36. Hucho, F. L., Oberthur, W. & Lottspeich, F. *FEBS Lett.* **205,** 137–142 (1986).
37. White, B. H. & Cohen, J. B. *J. biol. Chem.* **267,** 15770–15783 (1992).
38. Imoto, K. *et al. Nature* **335,** 645–648 (1988).
39. Charnet, P. *et al. Neuron* **2,** 497–513 (1990).
40. Imoto, K. *et al. FEBS Lett.* **289,** 193–200 (1991).
41. Villarroel, A., Herlitze, S., Koenen, M. & Sakmann, B. *Proc. R. Soc.* B**243,** 69–74 (1991).
42. Unwin, N. *Neuron* **3,** 665–676 (1989).
43. Lee, Y.-H. *et al. Biophys. J.* **66,** 646–653 (1994).
44. Galzi, J.-L. *et al. Nature* **359,** 500–505 (1992).
45. Eiselé, J.-L. *et al. Nature* **366,** 479–483 (1993).
46. Toyoshima, C. & Unwin, N. *Ultramicroscopy* **25,** 279–292 (1988).
47. Unwin, P. N. T. & Henderson, R. *J. molec. Biol.* **94,** 425–440 (1975).
48. Kubalek, E., Ralston, S., Lindstrom, J. & Unwin, N. *J. Cell Biol.* **105,** 9–18 (1987).
49. Sine, S. M. & Steinbach, J. H. *Biophys. J.* **46,** 277–284 (1982).

ACKNOWLEDGEMENTS. I thank A. Auerbach, F. Sachs, G. Hess and my colleagues at the MRC Laboratory and the Scripps Research Institute, La Jolla for helpful discussions and encouragement. The Marine Station, Roscoff, France, kindly supplied the *T. marmorata* for this work. The research was supported, in part, by grants from the NIH and the CEE.